The Astrophysical Journal Letters, 766:L17 (7pp), 2013 April 1 doi:10.1088/2041-8205/766/2/L17

WHAT DETERMINES THE DENSITY STRUCTURE OF MOLECULAR CLOUDS? A CASE STUDY OF ORION B WITH *HERSCHEL**

N. Schneider[1,2], Ph. André[1], V. Könyves[1,3], S. Bontemps[2], F. Motte[1], C. Federrath[4,5], D. Ward-Thompson[6], D. Arzoumanian[1,3], M. Benedettini[7], E. Bressert[8], P. Didelon[1], J. Di Francesco[9], M. Griffin[10], M. Hennemann[1], T. Hill[1], P. Palmeirim[1], S. Pezzuto[7], N. Peretto[1], A. Roy[1], K. L. J. Rygl[7], L. Spinoglio[7], and G. White[11,12]
[1] IRFU/SAp CEA/DSM, Laboratoire AIM CNRS, Université Paris Diderot, F-91191 Gif-sur-Yvette, France
[2] OASU/LAB-UMR5804, CNRS, Université Bordeaux 1, F-33270 Floirac, France
[3] IAS, CNRS/Université Paris-Sud 11, F-91405 Orsay, France
[4] MoCA, School of Mathematical Sciences, Monash University, VIC 3800, Australia
[5] Inst. für Theor. Astrophysik, Universität Heidelberg, D-69120 Heidelberg, Germany
[6] Jeremiah Horrocks Institute, UCLAN, Preston, Lancashire PR1 2HE, UK
[7] IAPS-INAF, Fosso del Cavaliere 100, I-00133 Roma, Italy
[8] CSIRO Astronomy and Space Science, Epping, Australia
[9] NRCC, Herzberg Institute of Astrophysics, University of Victoria, Canada
[10] University School of Physics and Astronomy, Cardiff, UK
[11] Department of Physics & Astronomy, The Open University, Milton Keynes MK7 6AA, UK
[12] RAL Space, Chilton, Didcot, Oxfordshire OX11 0NL, UK
Received 2012 December 30; accepted 2013 February 26; published 2013 March 13

ABSTRACT

A key parameter to the description of all star formation processes is the density structure of the gas. In this Letter, we make use of probability distribution functions (PDFs) of *Herschel* column density maps of Orion B, Aquila, and Polaris, obtained with the Herschel Gould Belt survey (HGBS). We aim to understand which physical processes influence the PDF shape, and with which signatures. The PDFs of Orion B (Aquila) show a lognormal distribution for low column densities until $A_V \sim 3$ (6), and a power-law tail for high column densities, consistent with a $\rho \propto r^{-2}$ profile for the equivalent spherical density distribution. The PDF of Orion B is broadened by external compression due to the nearby OB stellar aggregates. The PDF of a quiescent subregion of the non-star-forming Polaris cloud is nearly lognormal, indicating that supersonic turbulence governs the density distribution. But we also observe a deviation from the lognormal shape at $A_V > 1$ for a subregion in Polaris that includes a prominent filament. We conclude that (1) the point where the PDF deviates from the lognormal form does not trace a universal A_V -threshold for star formation, (2) statistical density fluctuations, intermittency, and magnetic fields can cause excess from the lognormal PDF at an early cloud formation stage, (3) core formation and/or global collapse of filaments and a non-isothermal gas distribution lead to a power-law tail, and (4) external compression broadens the column density PDF, consistent with numerical simulations.

Key words: dust, extinction – ISM: clouds – ISM: structure

Online-only material: color figures

1. INTRODUCTION

The star formation process represents a dramatic transformation of a molecular cloud in time and space where the main governing elements are turbulence, gravity, and magnetic fields. The spatial structure of clouds, now impressively revealed by *Herschel* imaging observations in the far-infrared (e.g., André et al. 2010; Motte et al. 2010; Molinari et al. 2010), is very inhomogeneous and dominated by filaments (Arzoumanian et al. 2011; Schneider et al. 2012). It is only with *Herschel Space Observatory* (Pilbratt et al. 2010) observations that diffuse to dense gas are now traced at high angular resolution (typically 18″). Combining PACS (Poglitsch et al. 2010) and SPIRE (Griffin et al. 2010) data provides column density maps that are superior to those obtained from extinction using near-IR data (Lombardi et al. 2006; Kainulainen et al. 2009; Froebrich & Rowles 2010; Schneider et al. 2011) that have angular resolutions of ≈2′ and suffer from saturation at visual extinctions A_V above ≈25.

Here, we aim to disentangle the relative contributions of turbulence, gravity, and external compression that influence the density structure of a molecular cloud. A useful analysis technique is to use probability distribution functions (PDFs) of the column density, which characterizes the fraction of gas with a column density N in the range $[N, N+\Delta N]$ (e.g., Federrath et al. 2010). Extinction maps (see above) have shown that molecular clouds can have a lognormal PDF for low column densities, and either a power-law tail or more complex shapes for higher column densities. Isothermal, hydrodynamic simulations including turbulence and gravity (e.g., Klessen et al. 2000) have shown that gravitational collapse induces a power-law tail in the PDF at high densities. More recent studies (Kritsuk et al. 2011; Federrath & Klessen 2013 and references therein) have investigated which parameters influence the shape of the PDF. Following these studies, fitting the slope of the high-density tail of the PDF allows us to determine the exponent α of an equivalent spherical density distribution $\rho(r) = \rho_0 (r/r_0)^{-\alpha}$.

In this study we make use of *Herschel*-derived column density PDFs of the Orion B molecular cloud, a template region for studies of low- to high-mass star formation (Lada et al. 1991). Orion B is amongst the nearest (distance ∼400 pc; Gibb 2008) giant molecular cloud complexes, with a mass of around $10^5\ M_\odot$, and hosts several OB-clusters (NGC 2023/24, NGC 2068/71). Orion B is located within the Hα-shell "Barnard's Loop" and diverse OB stellar aggregates impact the

* *Herschel* is an ESA space observatory with science instruments provided by European-led Principal Investigator consortia and with important participation from NASA.

cloud from the west with radiation and stellar winds. To understand better what governs the density structure and its link to star formation, we compare the Orion B PDFs to those obtained with the Herschel Gould Belt survey (HGBS) for a quiescent cloud (Polaris) and a star-forming region (Aquila).

2. OBSERVATIONS

Orion B, Aquila, and Polaris were observed with the PACS and SPIRE instruments on board *Herschel* as part of the HGBS (André et al. 2010) in parallel mode with a scanning speed of 60″ s^{-1} and two orthogonal coverages. The Orion B data were obtained on 2010 September 29 and 2011 March 13. For details on Polaris, see Men'shchikov et al. (2010), Miville-Deschênes et al. (2010), Ward-Thompson et al. (2010), and Könyves et al. (2010), and Bontemps et al. (2010) for Aquila. The angular resolutions at 160 μm (PACS), 250 μm, 350 μm, and 500 μm (all SPIRE) are ∼12″, ∼18″, ∼25″, and ∼36″, respectively. The SPIRE data were reduced with HIPE version 7.1956, including a destriper-module with a polynomial baseline of zeroth order. Both scan directions were then combined using the "naive-mapper," i.e., a simple averaging algorithm. The PACS data were reduced using HIPE 6.0.2106. In addition to the standard data reduction steps, non-linearity correction was applied on the 160 μm signal, which affects only the bright (>10 Jy pixel^{-1}) regime. The level1 data were then combined into a map with Scanamorphos v10 (Roussel 2012).

Column density and dust temperature maps were determined from a modified blackbody fit to the wavelengths 160–500 μm (see, e.g., Könyves et al. 2010). We recovered the *Herschel* zero-flux levels of the Orion B field for each wavelength with *Planck* data (Bernard et al. 2010). For the region covered by both PACS and SPIRE simultaneously, we fixed the specific dust opacity per unit mass (dust+gas) approximated by the power law $\kappa_\nu = 0.1\,(\nu/1000\ \mathrm{GHz})^\beta$ cm^2 g^{-1} and $\beta = 2$ (cf. Hildebrand 1983), took a mean molecular weight per hydrogen molecule of 2.8, and left the dust temperature and column density as free parameters. As an improvement to this procedure, we applied the technique described in Palmeirim et al. (2013) that uses the flux information of the 500 μm map but with the help of a multi-resolution decomposition, the angular resolution of the final maps is higher, i.e., that of the 250 μm data at 18″. To test the robustness of the derived high-resolution map of Orion B, we constructed ratio maps between the 18″ resolution column density map—smoothed to the common resolution of the 500 μm data (36″)—and the originally 36″ resolution maps. This ratio map has a mean value of 1.0 and a standard deviation of 0.03. The two column density maps agree within 15%. In addition, we investigated the effect of increasing opacity for high column densities (Roy et al. 2013) on the PDF and found that its dispersion decreases (∼10%–20%) and can provoke a steeper slope of the power-law tail for high densities.

Because the density structure of molecular clouds depends on how energy is injected into a cloud (spiral density waves, expanding supernovae shells, H II-regions, or gravitational contraction), we determine the hydrodynamic Mach number $\mathcal{M}$ that characterizes to first order the influence of turbulence. Stronger isothermal, non-magnetized supersonic turbulence leads to a higher Mach number and thus stronger local density enhancements. In contrast, magnetic fields smooth out density variations (Molina et al. 2012). $\mathcal{M}$ can be derived from observations of the FWHM (in km s^{-1}) of a molecular line, and the sound speed $c_s = 0.188\sqrt{T_{\rm kin}/10\ \mathrm{K}}$ with the kinetic temperature $T_{\rm kin}$:

$$\mathcal{M} = (\sqrt{3}\,\mathrm{FWHM})/(c_s\,\sqrt{8\ln 2}). \quad (1)$$

If the LTE assumption is valid, $T_{\rm kin} \approx T_{\rm ex}$, with $T_{\rm ex} = 5.53[\ln(5.53/T_{\rm mb}) + 1)]^{-1}$ for the optically thick ^{12}CO 1→0 line. If gas and dust are well mixed, the temperature should also correspond to the dust temperature derived from *Herschel*. We emphasize, however, that the determination of the Mach number remains rather uncertain (error ∼30%–40%) and mainly gives a *tendency*.

3. THE COLUMN DENSITY STRUCTURE OF ORION B

3.1. Column Density Maps

The column density map of Orion B (Figure 1) is dominated by the two active star-forming clumps NGC 2023/24 and NGC 2068/71 (Buckle et al. 2010) with very high local column densities $N(\mathrm{H_2})$ up to a few 10^{22} cm^{-2} and high dust temperatures of up to 35 K (Figure 2) due to the H II-regions. These two dense ridges are outlined by a column density level of ∼3–4 × 10^{21} cm^{-2} and stand out in an extended cloud with a typical column density of 1–2 × 10^{21} cm^{-2}. In contrast, the northern-eastern part of Orion B is colder and less active. A sharp cutoff in column density at the western border of NGC 2023/2024 and the Horsehead nebula is seen in column density cuts at constant declination (Figure 1) which was known from CO data (Wilson et al. 2005). From west to east, we first observe a strong increase of column density on a few pc scale for NGC 2023/2024, and a weaker but clearly visible increase for the southern region. East of the peaks, the column density decreases to a level of 1–2 × 10^{21} cm^{-2}, which is higher than the values at the western border. Such a profile was also seen in the Pipe nebula (Peretto et al. 2012) where the authors proposed a large-scale compression by the winds of the Sco OB2 association likely caused this sharp edge. A similar process may be at work for Orion B because the western part of the cloud is exposed to various OB aggregates (OB1b–d).

3.2. Probability Distribution Functions of Column Density

The distribution of number of pixels versus column density for Orion B, Aquila, and Polaris are displayed in Figure 4. We will use the term PDF and the notation $p(\eta)$ though the pure pixel distribution is not strictly a PDF which is defined for a lognormal distribution as

$$p(\eta)d\eta = \left(2\,\pi\,\sigma_\eta^2\right)^{-0.5}\,\exp\left[-(\eta-\mu)^2/\left(2\sigma_\eta^2\right)\right]d\eta, \quad (2)$$

with $\eta = \ln(N/\langle N\rangle)$ and σ_η as the dimensionless dispersion of the logarithmic field, and μ the mean. The normalization allows a direct comparison between clouds of different column density, and σ_η is a measure for the density variation in a turbulent medium. We determine σ_η with a fit to the assumed lognormal low-density part of the PDF and the slope with the index s from a power-law fit with $p(\eta) = p_0(\eta/\eta_0)^s$ to the high-density part. The results of the PDF fit are given together with the Mach number determination in Table 1.

The Orion B and Aquila PDFs show a well-defined lognormal part for low column densities and a clear power-law tail at higher column densities, starting at an extinction[13] $A_{\rm V}$ around

[13] For better comparison to the literature values, we use the visual extinction value derived from the column density adopting the conversion formula $N(\mathrm{H_2})/A_{\rm V} = 0.94 \times 10^{21}$ cm^{-2} mag^{-1} (Bohlin et al. 1978).

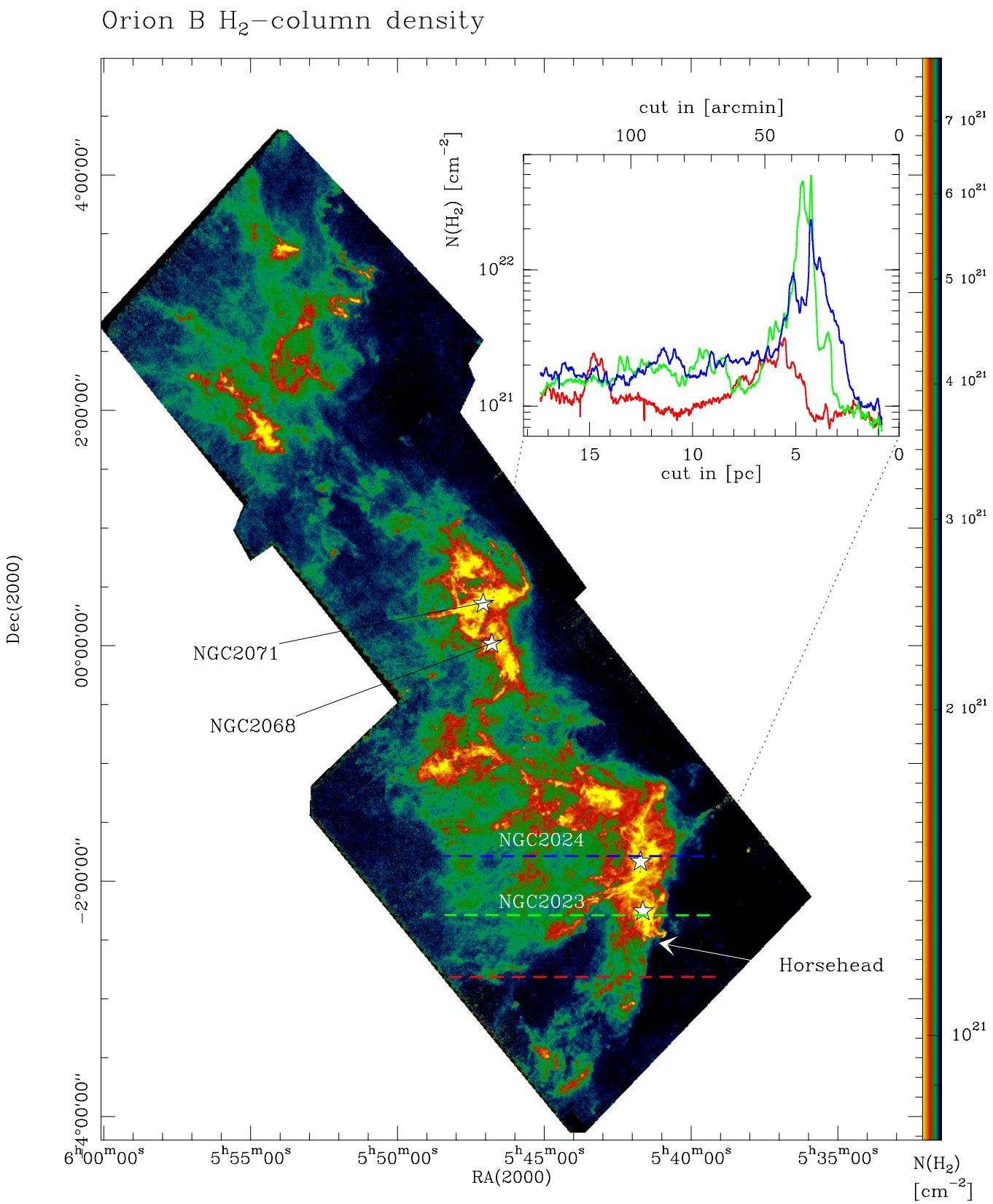

Figure 1. H_2-column density map at 18″ angular resolution of Orion B obtained from *Herschel* data. Known H II regions are labeled. The panel inside the image shows cuts (color-coded in blue, green, and red) in H_2-column density of the NGC 2023/24 region at constant declination. These cuts are indicated in the image.
(A color version of this figure is available in the online journal.)

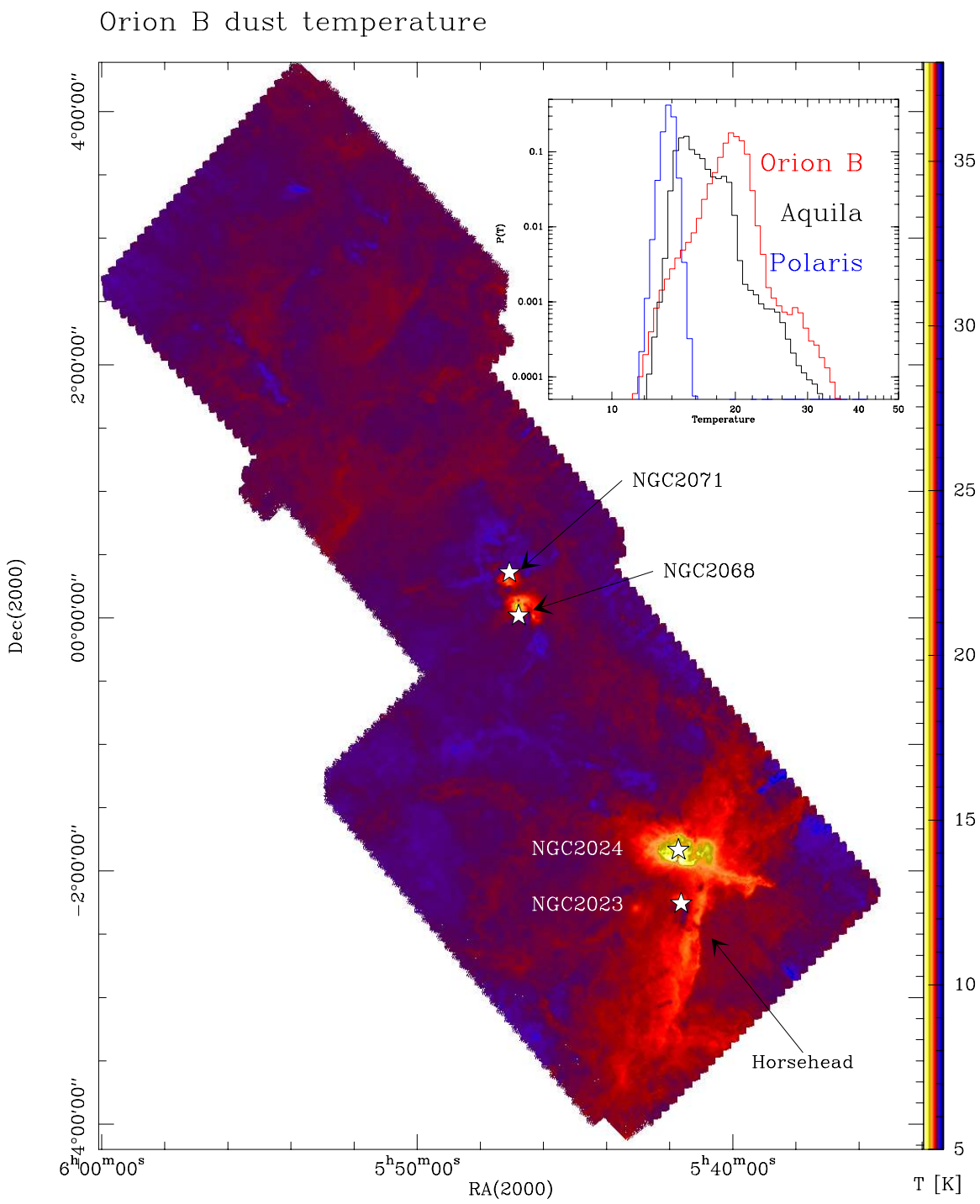

Figure 2. Dust temperature map at 18″ angular resolution of Orion B obtained from *Herschel* data. The panel inside the image shows the temperature PDFs of Orion B, Aquila, and Polaris (the whole region, not separated by subregions).

(A color version of this figure is available in the online journal.)

3 for Orion B and 6 for Aquila. To first order, the PDFs only differ in their width ($\sigma_\eta = 0.45$ for Orion B and 0.3 for Aquila). The PDFs of two subregions (Figure 3) in the Polaris cirrus cloud (Falgarone et al. 1998) are more narrow with $\sigma = 0.22$ and 0.27, respectively. The PDF of the quiescent region is almost perfectly lognormal; however, above $A_V \sim 1.5$ we observe a slight excess which is most likely a resolution effect but may possibly result from a physical process (see Section 3.3). A clear deviation from the lognormal shape is found for the "saxophone" filament. Interestingly, the excess for $A_V > 1$ has not the form of a power-law tail. Note that all PDF features (shape, width, etc.) do not depend on the angular resolution (18″ versus 36″) or pixel number (our statistic here is high because the images are on a 6″ grid). To quantify better the deviation of the PDF from lognormal, we determined the higher moments[14] skewness $\mathcal{S}$ and kurtosis $\mathcal{K}$. The skewness, describing the asymmetry of the distribution, is positive for Orion B, Aquila, and

[14] $\mathcal{S} = (1/\sigma^3)\int_{-\infty}^{\infty} d\eta\, p(\eta)[\eta - \langle\eta\rangle]^3$ and $\mathcal{K} = (1/\sigma^4)\int_{-\infty}^{\infty} d\eta\, p(\eta)[\eta - \langle\eta\rangle]^4$ (see, e.g., Federrath et al. 2010).

Table 1
Temperature Regime, Mach Number, and PDF Fit Results for Orion B, Aquila, and Polaris

Cloud	T_{ex}(CO) (K) (1)	T_{dust} (K) (2)	$\langle T_{ex}\rangle$(CO) (K) (3)	$\langle T_{dust}\rangle$ (K) (4)	Δv (km s^{-1}) (5)	$\mathcal{M}$ (6)	σ_η (7)	α (8)
OrionB	5–70	5–45	20	16	~3	~8	0.45	1.99
Aquila	···	9–40	20	19	~2.2	~6	0.30	1.77
Polaris-quiet	···	12–15	10	13	~1	~3	0.22	···
Polaris-saxophone	~10–15	11–14	12	13	~2	~7	0.27	···

Notes.
(1) Observed excitation temperature range from ^{12}CO 1→0 data (Orion B: Buckle et al. 2010; Aquila: Zeilik et al. 1978; Polaris: Bensch et al. 2003; Shimoikura et al. 2012). No large-scale CO data are available for Polaris and Aquila).
(2) Observed dust temperature range from *Herschel* data.
(3) and (4) Average temperature.
(5) Line width from ^{12}CO 1→0.
(6) Sonic Mach number from average temperature and CO line width.
(7) Dispersion of the PDF.
(8) Exponent of the spherical density profile.

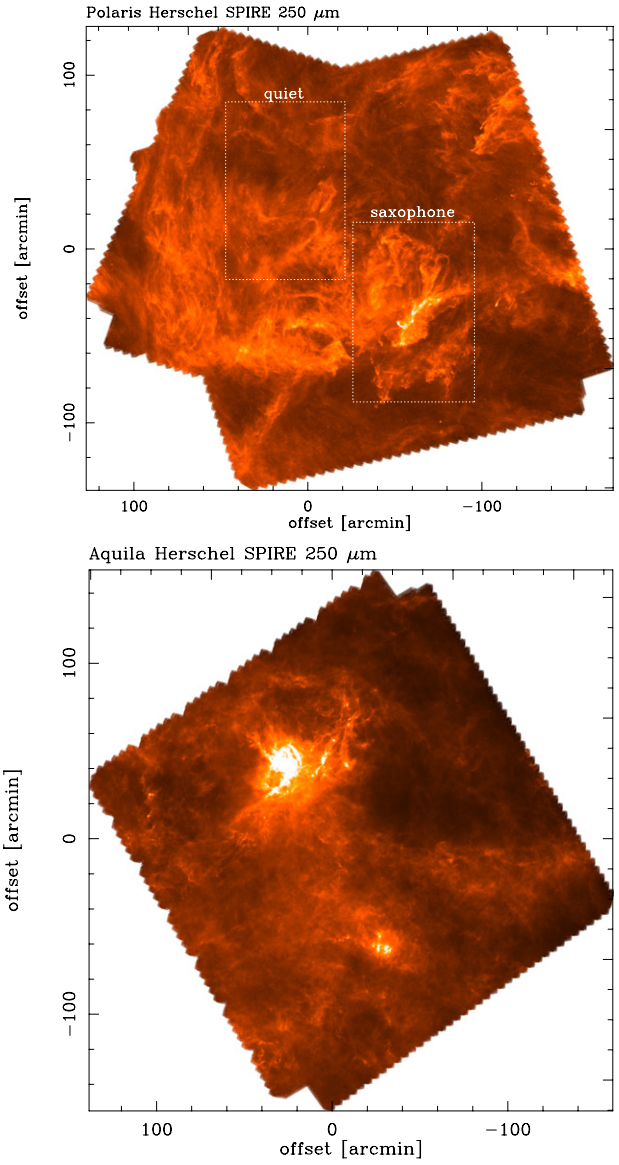

Figure 3. *Herschel* SPIRE map at 250 μm of the Polaris and Aquila fields. The two regions for which we show the corresponding column density PDFs for Polaris are indicated by dashed white lines. These are the "saxophone," a region containing a filament with high column density but lacking star formation and a subregion further northeast.

(A color version of this figure is available in the online journal.)

Polaris-saxophone ($\mathcal{S}$ = 1.17, 1.24, and 0.49, error typically 0.05), implying an excess at higher column densities, and is $\mathcal{S}$ = 0.19 ($\mathcal{K}$ = 3.0) for Polaris-quiet, confirming the nearly lognormal form of its PDF. The Orion B and Aquila PDFs have much higher values for the kurtosis ($\mathcal{K}$ = 6.8 and 7.9) that arise from pronounced wings. The Polaris-saxophone region has also a (high) value of $\mathcal{K}$ = 4.4, indicating an excess at high column densities.

From theory, a purely lognormal distribution is only expected if the cloud structure is shaped by supersonic, isothermal turbulence, while deviations in the form of a power law for high column densities are predicted for self-gravitating clouds (Klessen et al. 2000; Ballesteros-Paredes et al. 2011). The concept of isothermality does not fully apply to all clouds, as can be seen in the temperature PDFs in Figure 2. While Polaris can be considered as a nearly isothermal gas phase, Orion B and Aquila show a more complex temperature distribution over a larger range. Froebrich & Rowles (2010) argued that the A_V-value where the transition of the PDF must take place is always around 6, and defined this value as a threshold for star formation. Kainulainen et al. (2011) found values between A_V = 2 and 5 and proposed a scenario in which this A_V-range marks a transition between dense clumps and cores and a more diffuse interclump medium. The PDFs of Orion B and Aquila shown in Figure 4 clearly show that the transition from lognormal to power law is not universal but varies between clouds ($A_V \sim 3$ and 6, respectively). This behavior suggests that the A_V -transition value neither represents a universal threshold in star formation nor a phase transition (unless the density of the clumps and the interclump medium strongly varies from cloud to cloud). A similar result was obtained in the study of N. Schneider et al. (2013, in preparation), presenting a large sample of PDFs from low- to high-mass star-forming clouds. Deviations of the PDF from lognormal are more likely a function of cloud parameters, in particular the virial parameter, the dominant forcing mode,[15] and the Mach number as shown in models (Federrath & Klessen 2013) and observations (N. Schneider et al. 2013, in preparation).

From the slope of the power-law tail for Orion B and Aquila, the exponent of an equivalent spherical density distribution

[15] *Compressive* modes on large to small scales are generated by galactic spiral shocks, expanding supernova shells and H II regions, gravitational contraction, and outflows. *Solenoidal* forcing arises from galactic rotation and magneto-rotational instabilities.

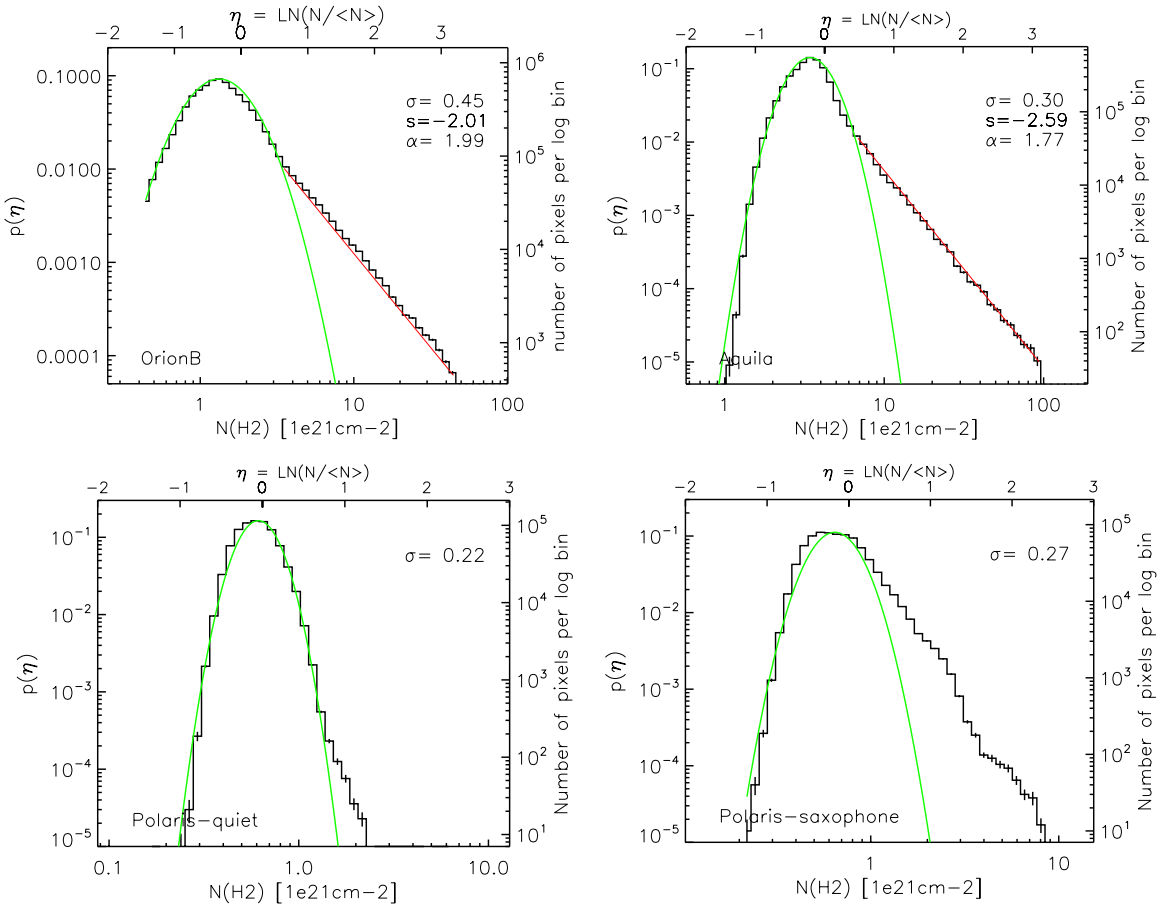

Figure 4. Probability distribution functions of column density for Orion B and Aquila (top) and Polaris (bottom) at an angular resolution of 18″ (a similar version of the Aquila PDF was previously shown in André et al. 2011). The left *y*-axis is the PDF as a normalized probability $p(\eta)$, while the right *y*-axis indicates the number of pixels per logarithmic bin. Note that due to the large number of pixels (6″ grid), the error bars calculated using Poisson statistics are very small. The PDFs do not change using a lower sampled grid (i.e., at the resolution of 18″ or 36″). The lower *x*-axis gives the column density $N(H_2)$ in units of 10^{21} cm^{-2} (corresponding approximately to the A_V in magnitudes using the Bohlin factor). The upper *x*-axis is the dimensionless parameter $\eta = \ln(N/\langle N\rangle)$. The green curve indicates the fitted lognormal PDF and the red line the power-law fit to the high-density tail. The width of the fitted lognormal PDF (σ_η), the power-law slope index *s*, and the exponent α of the equivalent spherical density profile ($\rho \propto r^{-\alpha}$) are given in each panel. Note that the variation of opacity with density causes a systematic error on the PDF which is larger than the statistical error. We estimate the error on σ and α to be typically 10%–20%.

(A color version of this figure is available in the online journal.)

$\rho(r) \propto r^{-\alpha}$ is determined to be $\alpha = 1.99$ (1.77) for Orion B (Aquila), conforming with results typically obtained for individual collapsing cores. The high-density tail, however, cannot be explained by the core population alone because it does not provide sufficient mass (Könyves et al. 2010). Moreover, it is probably also caused by global gravitational collapse of larger spatial areas like filaments and ridges (see, e.g., Schneider et al. 2010; Hill et al. 2011; Palmeirim et al. 2013 for observational examples). It was shown that non-isothermal flows can also cause power-law tails (Passot & Vazquez-Semadeni 1998) so that this process may influence the shape of the PDF as well. Indeed, in regions with significant temperature variations, α can reach values larger than free fall ($\alpha = 2.4$ for the high-mass star-forming cloud NGC 6334; Russeil et al. 2013), possibly pointing toward a scenario in which heating/cooling processes become important.

3.3. Comparison to Models

We compare our observational PDFs with those obtained from hydrodynamic simulations (Federrath & Klessen 2013), including gravity, magnetic fields, and different turbulent states ($\mathcal{M}$ = 2–50, star formation efficiencies from 0% to 20%, and different forcing modes). In addition, we determine the "*b*-parameter" ($\sigma_s^2 = f^2\,\sigma_\eta^2 = \ln(1 + b^2\,\mathcal{M}^2)$, e.g., Federrath et al. 2010; Burkhart & Lazarian 2012), characterizing the link between density and velocity in a cloud. We find the following.

1. The dispersion σ_η of the PDF for Aquila is 0.3 and for the two Polaris subregions 0.22 and 0.27, while $\sigma_\eta = 0.45$ for Orion B. At the same time, the Mach number for all regions is typically 6–8 (in view of the uncertainty of $\mathcal{M}$, they are basically the same), while only the Polaris-quiet subregion has a significant lower value of 3. Numerical models indicate that a larger width is caused by a higher Mach number and/or compressive forcing instead of solenoidal forcing (see also Federrath et al. 2010; Tremblin et al. 2012). Since Orion B and Aquila have similar values of Mach number, we conclude that the Orion B cloud is likely exposed to compressive modes—as seen also in the sharp cutoff of column density (Figure 1)—caused by the stellar winds from diverse OB aggregates.[16] Aquila has been proposed to be located at an encounter of several superbubbles (Frisch

[16] Note that the Pipe cloud as a clear example of compression (Section 3.1) also shows a broad PDF with $\sigma_\eta = 0.60$ in extinction maps (N. Schneider et al. 2013, in preparation).

1998), but the impact on its density structure—more or less important than close-by OB-stars—cannot be inferred. Both clouds are exposed to relatively high magnetic fields (Crutcher et al. 1999; Sugitani et al. 2011), so that the more narrow PDF of Aquila is presumably not caused by magnetic fields alone.

2. Polaris-quiet has a narrow ($\sigma = 0.22$), lognormal PDF, the gas is nearly isothermal (see temperature PDF in Figure 2), and has a low (~3) Mach number. Only isothermal turbulence simulations without self-gravity reproduce this shape of the PDF. We computed the forcing parameter $b = 1/\mathcal{M} \times (\exp((f\,\sigma_\eta)^2) - 1)^{0.5}$ using an average of 2.5 between solenoidal and compressive forcing (Federrath et al. 2010) for the factor $f = \sigma_s/\sigma_\eta$ (estimation of the three-dimensional density fluctuation σ_s out of the two-dimensional column density fluctuation σ_η). The resulting value of $b = 0.2$ is lower than what was found by comparing with the purely solenoidal driven isothermal MHD simulations of Burkhart & Lazarian (2012). Our data point for Polaris-quiet fits on their model (Figure 3) with $b = 1/3$. In any case, these results show that the Polaris-quiet PDF is consistent with the view that the cloud's density distribution is mainly governed by solenoidal forcing.
3. Power-law tails in the high-density PDF regime form under the presence of self-gravity, but can also be provoked by purely non-isothermal turbulence (Passot & Vazquez-Semadeni 1998). For Orion B and Aquila, gravity most likely dominates because a large number of prestellar and protostellar dense cores and supercritical filaments are present (André et al. 2010; V. Könyves et al., in preparation). The gas is not isothermal (Figure 2), but the temperature does not vary by several orders of magnitude either. The excess in the PDF for the Polaris-saxophone region is more difficult to interpret. In this gravitational and thermally subcritical filament, only one candidate prestellar core (Ward-Thompson et al. 2010; Shimoikura et al. 2012) was found. The gas can be considered as isothermal, so that here magnetic fields may play a role (the strength is not known), leading to a narrow PDF (e.g., Molina et al. 2012), or statistical density fluctuations and intermittency due to locally compressive turbulence. These effects may also explain the slight excess in the PDF of Polaris-quiet.

SPIRE has been developed by a consortium of institutes led by Cardiff Univ. (UK) and including Univ. Lethbridge (Canada); NAOC (China); CEA, LAM (France); IFSI, Univ. Padua (Italy); IAC (Spain); Stockholm Observatory (Sweden); Imperial College London, RAL, UCL-MSSL, UKATC, Univ. Sussex (UK); and Caltech, JPL, NHSC, Univ. Colorado (USA). This development has been supported by national funding agencies: CSA (Canada); NAOC (China); CEA, CNES, CNRS (France); ASI (Italy); MCINN (Spain); SNSB (Sweden); STFC, UKSA (UK); and NASA (USA). We thank J.-Ph. Bernard for providing the flux values from *Planck*. C. Federrath acknowledges the Australian Research Council for a Discovery Projects Fellowship (grant No. DP110102191). Part of this work was supported by the ANR-11-BS56-010 project "STARFICH."

REFERENCES

André, Ph., Men'shchikov, A., Bontemps, S., et al. 2010, A&A, 518, L102
André, Ph., Men'shchikov, A., Könyves, V., & Arzoumanian, D. 2011, in IAU Symp. 270, Computational Star Formation, ed. J. Alves et al. (Cambridge: Cambridge Univ. Press), 255
Arzoumanian, D., André, Ph., Didelon, P., et al. 2011, A&A, 529, L1
Ballesteros-Paredes, J., Vázquez-Semaedi, E., Gazol, A., et al. 2011, MNRAS, 416, 1436
Bensch, F., Leuenhagen, U., Stutzki, J., et al. 2003, A&A, 591, 1013
Bernard, J.-P., Paradis, D., Marshall, D. J., et al. 2010, A&A, 518, L88
Bohlin, R. C., Savage, B. D., & Drake, J. F. 1978, ApJ, 224, 132
Bontemps, S., André, P., Könyves, A., et al. 2010, A&A, 518, L85
Buckle, J., Curtis, E., Roberts, J., et al. 2010, MNRAS, 401, 204
Burkhart, B., & Lazarian, A. 2012, ApJL, 755, L19
Crutcher, R. M., Roberts, D. A., Troland, T. H., et al. 1999, ApJ, 515, 275
Falgarone, E., Panis, F.-F., Heithausen, A., et al. 1998, A&A, 331, 669
Federrath, C., & Klessen, R. S. 2013, ApJ, 763, 51
Federrath, C., Roman-Duval, J., Klessen, R. J., et al. 2010, A&A, 512, 81
Frisch, P. C. 1998, in Proc. IAU Colloq. 166, The Local Bubble and Beyond, ed. D. Breitschwerdt, M. J. Freyberg, & J. Truemper (Berlin: Springer), 269
Froebrich, D., & Rowles, J. 2010, MNRAS, 406, 1350
Gibb, A. 2008, in Handbook of Star Forming Regions, Vol. I, ed. B. Reipurth (San Francisco, CA: ASP), 693
Griffin, M., Abergel, A., Abreau, A., et al. 2010, A&A, 518, L3
Hildebrand, R. H. 1983, QJRAS, 24, 267
Hill, T., Motte, F., Didelon, P., et al. 2011, A&A, 533, 94
Kainulainen, J., Beuther, H., Banerjee, R., et al. 2011, A&A, 530, 64
Kainulainen, J., Beuther, H., Henning, T., & Plume, R. 2009, A&A, 508, L35
Klessen, R. S. 2000, ApJ, 535, 869
Könyves, V., André, P., Men'shchikov, A., et al. 2010, A&A, 518, L106
Kritsuk, A. G., Norman, M. L., & Wagner, R. 2011, ApJL, 727, L20
Lada, E. A., Evans, N. J., II, DePoy, D. L., et al. 1991, ApJ, 371, 171
Lombardi, M., Alves, J., & Lada, C. 2006, A&A, 454, 781
Men'shchikov, A., André, P., Didelon, P., et al. 2010, A&A, 518, L103
Miville-Deschênes, M.-A., Martin, P., Abergel, A., et al. 2010, A&A, 518, L104
Molina, F., Glover, S., Federrath, C., & Klessen, R. 2012, MNRAS, 423, 2680
Molinari, S., Swinyard, B., Bally, J., et al. 2010, A&A, 518, L100
Motte, F., Zavagno, A., Bontemps, S., et al. 2010, A&A, 518, L77
Palmeirim, P., André, Ph., Kirk, J., et al. 2013, A&A, 550, 38
Passot, T., & Vazquez-Semadeni, E. 1998, PhRv, 58, 4501
Peretto, N., André, Ph., Könyves, V., et al. 2012, A&A, 541, 63
Pilbratt, G., Riedinger, J., Passvogel, T., et al. 2010, A&A, 518, L1
Poglitsch, A., Waelkens, C., Geis, N., et al. 2010, A&A, 518, L2
Roussel, H. 2012, PASP (arXiv:1205.2576)
Roy, A., Martin, P., Polychroni, D., et al. 2013, ApJ, 763, 55
Russeil, D., Schneider, N., Anderson, L., et al. 2013, A&A, submitted
Schneider, N., Bontemps, S., Simon, R., et al. 2011, A&A, 529, 1
Schneider, N., Csengeri, T., Bontemps, S., et al. 2010, A&A, 520, 49
Schneider, N., Csengeri, T., Hennemann, M., et al. 2012, A&A, 540, L11
Shimoikura, T., Dobashi, K., Sakurai, T., et al. 2012, ApJ, 745, 195
Sugitani, K., Nakamura, F., Watanabe, M., et al. 2011, ApJ, 734, 63
Tremblin, P., Audit, E., Minier, V., et al. 2012, A&A, 546, 33
Ward-Thompson, D., Kirk, J., André, Ph., et al. 2010, A&A, 518, L92
Wilson, B., Dame, T., Masheder, M., et al. 2005, A&A, 430, 523
Zeilik, M., & Lada, C. 1978, ApJ, 222, 896